CNWRA *A center of excellence in earth sciences and engineering™*

Geosciences and Engineering Division
6220 Culebra Road • San Antonio, Texas, U.S.A. 78238-5166
(210) 522-5160 • Fax (210) 522-5155

June 26, 2008
Contract No. NRC–02–07–006
Account No. 14002.01.151
WM–00011

ATTN: Document Control Desk
U.S. Nuclear Regulatory Commission
Mr. Eugene Peters
Office of Nuclear Material Safety and Safeguards
Division of High-Level Waste Repository Safety
Two White Flint North
11545 Rockville Pike
Mail Stop EBB-2-BO2
Washington, DC 20555

Subject: Draft–Understanding Eruption Dynamics of Yucca Mountain Region Volcanoes: Textures of Eruption Products From Lathrop Wells Cinder Cone (Intermediate Milestone No. 14002.01.151.801)

Dear Mr. Peters:

This letter transmits Intermediate Milestone 20.14002.01.151.801, Draft–Understanding Eruption Dynamics of Yucca Mountain Region Volcanoes: Textures of Eruption Products From Lathrop Wells Cinder Cone. In this summary letter report, CNWRA staff investigated the dynamics of magma ascending in a volcanic conduit by systematically studying the vesiculation and crystallization textures in eruptive products from Lathrop Wells volcano, southern Nevada. As magma ascends in a dike/conduit, volatile exsolution occurs which causes rapid crystal nucleation, both of which affect the physical properties of the magma and the conditions of flow. The eruption of Lathrop Wells volcano is considered an analog to possible future activity that might disturb the potential underground repository at Yucca Mountain; by examining bubble and crystal populations in Lathrop Wells scoria that represents the activity through time, changes in dike/conduit development and flow regimes can be discerned and applied to evaluations of uncertainties in performance assessment models. This work provides a more integrated understanding of the processes that occur during a violent Strombolian eruption, which can be translated to models used to examine possible consequences of igneous activity.

Washington Office
1801 Rockville Pike, Suite 105 • Rockville, Maryland 20852-1633

If you have any questions on this deliverable, please contact Philippe Dubreuilh at 210-522-5085 or at pdubreuilh@swri.org.

Sincerely,

Philippe Dubreuilh, Ph.D.
Manager, Geology & Geophysics

PD/slo
Attachment
cc:

NRC
L. Kokajko
B. Meehan
D. DeMarco
S. Kim
A. Mohseni
J. Davis
M. Shah
B. Hill
T. McCartin
K. Stablein
J. Rubenstone
J. Guttmann
S. Whaley
P. Justus
B. Brooks

CNWRA/GED
W. Patrick (letter only)
B. Sagar (letter only)
N. Adams
CNWRA Dirs/EMs (letter only)
L. Gutierrez (letter only)

SwRI
Record Copy B, IQS

UNDERSTANDING ERUPTION DYNAMICS OF YUCCA MOUNTAIN REGION VOLCANOES: TEXTURES OF ERUPTION PRODUCTS FROM LATHROP WELLS CINDER CONE

Prepared for

U.S. Nuclear Regulatory Commission
Contract NRC–02–07–006

Prepared by

Nancy Adams

Center for Nuclear Waste Regulatory Analyses
San Antonio, Texas

June 2008

CONTENTS

FIGURES

ACKNOWLEDGMENTS

This report was prepared to document work performed by the Center for Nuclear Waste Regulatory Analyses (CNWRA®) and its contractors for the U.S. Nuclear Regulatory Commission (NRC) under Contract Nos. NRC–02–02–012 (fiscal year 2007) and NRC–02–07–006 (fiscal year 2008). The activities reported here were performed on behalf of the NRC Office of Nuclear Material Safety and Safeguards, Division of High-Level Waste Repository Safety. This report is an independent product of CNWRA and does not necessarily reflect the views or regulatory position of NRC.

The author thanks A. Morris for technical review, G. Wittmeyer for programmatic review, and L. Mulverhill for editorial review of this report. The author also appreciates S. Odam for providing word processing support in the preparation of this document. Additional thanks go to D. Waiting for producing field maps and Figure 1 and M. Silver, S. Biswas, and S. Rubio for field and lab assistance. Finally, the author wishes to acknowledge D. Olmos and S. Birnbaum at the University of Texas at San Antonio for their scanning electron microscope help.

QUALITY OF DATA, ANALYSES, AND CODE DEVELOPMENT

DATA: All CNWRA-generated original data contained in this report meet quality assurance requirements described in the Geosciences and Engineering Division Quality Assurance Manual. Sources of other data should be consulted for determining the level of quality of those data. The work presented in this report is documented in Scientific Notebook 870E.

ANALYSES AND CODES: No specialized or controlled software was used in this report.

1 INTRODUCTION

1.1 Background

The potential high-level nuclear waste repository at Yucca Mountain, Nevada, is located within a geologically active basaltic volcanic field that includes eight cinder cones formed since 1 Ma within a 50-km [31-mi] radius (Fleck, et al., 1996; Heizler, et al., 1999). Given the location and thus the potential for volcanic activity to disrupt waste packages and transport radionuclides to the surface, possible future igneous activity may need to be included in any postclosure performance assessments. The risk of igneous activity to repository performance is captured by the potential consequences of an igneous intrusion or volcanic conduit intersecting and damaging waste packages and the probability that an igneous event will occur. Currently, U.S. Department of Energy (DOE) adopts a mean of 1.7×10^{-8} for the annual frequency of a basaltic dike intersecting the repository (Bechtel SAIC Company, LLC, 2004). Because the probability is $>10^{-8}$/yr, according to U.S. Nuclear Regulatory Commission (NRC) regulations for disposal of high-level radioactive waste at Yucca Mountain (10 CFR Part 63), volcanic hazard analyses must be included in the DOE performance assessment. In addition to the probability, the other key component that factors into the risk analysis is the potential consequences of magma–repository interactions. To model the effects of rising basaltic magma on subsurface drifts, waste packages, and drip shields, the dynamics occurring in a volcanic conduit that govern the conditions inside the drift upon intersection must be understood.

Textures of eruption products, specifically clast morphology, clast density, vesicle size and shape, and microlite crystallinity, can be used to study magma-ascent dynamics occurring in a conduit/dike. As a water-rich magma ascends in a volcanic conduit/dike, degassing and crystallization processes can occur depending on ascent rate. At some depth determined by composition, a magma becomes saturated in volatiles, which exsolve with continued decompression. Exsolution of dissolved volatiles, specifically water, from the melt increases the liquidus temperature and drives the crystallization of tiny crystals called microlites. The decreasing concentration of volatiles and the nucleation and growth of vesicles (gas) and microlites (solid) induce changes in melt rheology, which is critically linked to eruptive style and flow regime (Cashman, 2004). For example, if bubble growth rate and magma ascent rate outstrip bubble rise rate, exsolution reaches a critical threshold and the magma fragments, resulting in explosive-style eruptions. If gas can escape from the magma freely either by an interconnected bubble network or by a bubble rise rate greater than a magma ascent rate, the magma may reach the surface without fragmenting and erupt effusively (Cashman, et al., 2000). Thus, the complex interplay between flow variables and magma properties, none of which remain static as magma rises from the chamber toward the surface, is linked to microlite and bubble nucleation events, and the resulting microtextures are a record of these events as well as bubble growth by diffusion, decompression, and coalescence, and bubble collapse and can be used to discern conditions inside the conduit/dike during ascent.

Using pyroclastic microtextures to study conduit dynamics applicable to potential future eruptions at Yucca Mountain entails examining products from an appropriate analog eruption in terms of style, intensity, and composition. Based on the volcanic history of the region, a future event is likely to involve effusion of lava flows and Strombolian–violent Strombolian eruptions and construction of a monogenetic, basaltic scoria cone. Considering its state of preservation, proximity to the proposed repository footprint {~18 km [11 mi] south}, composition, and age, Lathrop Wells volcano provides a good example of the type of eruptive event that could disrupt the repository. The ~80 ka eruption of water-rich [~1.2–4.6 wt% H_2O (Luhr and Housh, 2002; Nicholis and Rutherford, 2004)] trachybasalt was characterized by both effusive and explosive

activity, resulting in two lava flow fields, fall deposits, and a 140-m [459-ft]-high scoria cone (Sandia National Laboratories, 2007). Field observations suggest the emplacement of these three types of deposits overlapped in time. Excavation of the cone through commercial quarrying has provided access to eruptive products that represent the duration of the cone-building process, and two distinct facies have been observed. The lower cone facies consists of partly welded coarse lapilli and bombs indicative of Strombolian explosions along a short fissure that occurred simultaneously with effusion of south flow field lavas. As the eruption continued, activity became increasingly energetic and focused from a fissure to a vent that at times supported a sustained eruption column, and the bulk of the cone was built. This upper cone facies is composed of nonwelded beds of vesicular scoria lapilli, consistent with the increase in eruption intensity and degree of fragmentation that characterizes violent Strombolian activity (Valentine, et al., 2007). The upper-cone-building activity was accompanied by the emplacement of fall deposits and the effusion of the northeast lava flow field.

1.2 Purpose and Scope

In performance assessments DOE, NRC, and Center for Nuclear Waste Regulatory Analyses (CNWRA®) conducted for the proposed high-level waste repository at Yucca Mountain, Nevada, risk associated with a volcanic disruptive event is directly proportional to the number of waste packages that is considered to have failed. The number of failed waste packages is largely determined by the conduit-diameter parameter in the volcanic scenario model abstraction. Studying the development and evolution of a conduit during a volcanic eruption can assist in its parameterization as well as the evaluation of the assumptions and uncertainties inherent in the parameterization. Understanding the processes that occur as magma ascends in a conduit is also important to assessing consequences related to intersections between a conduit/dike and a drift and interactions between intruding magma and the engineered barrier system.

CNWRA conducted field and laboratory investigations of volcanics from the Lathrop Wells scoria cone to gain a better understanding of conduit dynamics during a potential future volcanic event with the style, composition, and intensity most likely to disrupt the potential repository site. Given that the major element composition changed very little throughout the course of this eruption (Valentine, et al., 2007), fluid dynamic processes associated with the exsolution of volatiles during magma ascent apparently greatly affected the eruptive behavior. Different deposit types (e.g., lava flows, fall deposits, cone deposits) as well as variations within individual deposits demonstrate behavioral changes on multiple scales and the overall complexity of the eruption, and much of this complexity can be attributed to processes of vesiculation and crystallization occurring in the conduit. To discern the conditions that favor different dominant processes, this study focused primarily on pyroclasts collected from the cone deposits. The degree of welding and fragmentation seen in the cone deposits indicates eruption styles ranging from fire-fountaining to violent Strombolian, and the size of clasts available for sampling ensures a quantifiable number of bubbles and microlites across a range of sizes that represent different stages of nucleation and growth. Thus, the scope of this project was to use pyroclastic textures present in the cone deposits of Lathrop Wells volcano, an appropriate analog to a potential future disruptive volcanic event at Yucca Mountain, with the objective of characterizing conditions of magma ascent in a conduit so that models and consequences of eruptions can be evaluated.

2 METHODOLOGY

2.1 Sampling

The Lathrop Wells volcano consists of a scoria cone {0.02 km^3 [2.6 $\times$ 10^7 yd^3]} with a north-south elongated base and a summit crater, two lava flow fields {0.03 km^3 [3.9 $\times$ 10^7 yd^3]}, and a fall deposit {0.07 km^3 [9.2 $\times$ 10^7 yd^3]} (Valentine, et al., 2007, 2005). One lava flow field extends near the base of the cone toward the south and is covered by fallout and mounds of pyroclastic material rafted from the cone; the other flowed northeastward and then south and proximally is overlain by some pyroclastic mounds and fallout, but distally it overlies fall deposits (Figure 1)[1]. The fall deposits, which with the exception of deposits proximal to the cone have been largely eroded or buried by alluvium, consist of well-fragmented, highly vesicular basalt lapilli and ash. Samples were collected from both lava flow fields, pyroclastic mounds on the south lava flow, and fall deposits, but for this study, sampling focused primarily on the cone deposits.

Valentine, et al. (2007, 2005) divide the cone deposits into two distinct facies: (i) the early/lower cone facies of agglutinate with abundant spindle and ribbon bombs and (ii) the later/upper cone facies of highly vesicular, well-sorted, nonagglutinated lapilli-sized scoria. Exposures of the lower cone deposit are transient and dependent on quarrying operations, but lower cone beds as well as a distinct contact between the lower and upper cone were exposed in May 2007 (Figure 2). Samples of individual beds in both facies were collected from the base of the cone to the summit. Inversely graded horizons in the upper cone indicate grain avalanching occurred as the cone grew, but beds exposed in quarry cuts near the base of the cone were deposited earlier in the eruption than beds located near the top. Samples were collected from narrow vertical intervals, and the locations were chosen based on variations in clast size and character that represent transitions and/or pulses in activity that occurred during cone construction. Each consisted of approximately 50–100 clasts of scoria 8–32 mm [0.3–1.3 in] in diameter. Twenty-one samples were collected in total, 4 from the lower cone and 17 from the upper cone.

2.2 Density

Density was measured on each clast from the 21 samples collected from the cone and 2 samples collected from the fall deposits by the method described in Houghton and Wilson (1989). Bulk vesicularity for each clast was also determined using a dense rock equivalent density of 2.65 g/cm^3 [165.4 lb/ft^3]. Density distributions were examined for each of the 21 samples, and considering variations in the cone sample distributions with cone height, 9 samples were selected, from which polished thin sections were made from specific clasts. Subsets of two to six clasts from each selected sample were used to produce the thin sections, and these were targeted based on their density and macroscopic textures. One thin section was also produced from a fall deposit clast for comparison.

2.3 Image Analysis

Microscopic pyroclastic textures are defined by vesicle size and shape and microlite abundance and assemblage. These features can be analyzed in images captured from thin sections at various magnifications. In this study, to characterize the heterogeneity in vesicle and microlite populations seen in a single thin section, resolutions of the digital images required for textural characterization ranged from 50–5,000 pixels/mm [1,270–1.3 $\times$ 10^5 pixels/in] (lowest to highest

[1] All figures have been placed at the end of this document for easier reference.

magnification). The lowest magnification images were collected by scanning the thin sections on a Hewlett-Packard flatbed scanner at 1,200 dpi resolution {50 pixels/mm [1,270 pixels/in]}. Backscatter electron images with a resolution of 72 dpi were collected using a JEOL-840A scanning electron microscope operating at a 20 kV accelerating voltage and a 1-nA beam current for the higher magnifications. Higher magnification images were collected from areas that represent the range of vesicle and microlite populations present in the entire thin section; therefore, images were not centered over large phenocrysts or bubbles. For each thin section, nested sets of higher magnification images were acquired. A minimum of two 120 pixels/mm [3,048 pixels/in] images were taken, and within these images, additional images were taken at a slightly higher magnification {usually at 500 pixels/mm [1.3×10^4 pixels/in]}, and within these images, still higher magnification images were captured {up to 5,000 pixels/mm [1.3×10^5 pixels/in]}. Between 9 and 24 images were acquired for each of the 24 thin sections produced. Images were captured in grayscale; in the images taken using the flatbed scanner, glass and crystals are gray to black and vesicles are white, and in the higher magnification images taken using the scanning electron microscope, glass and crystals are gray to white and vesicles are black.

3 RESULTS

3.1 Density

Density was measured on clasts comprising the 21 cone samples and 2 samples collected from the fall deposits. For each of the cone samples, a histogram showing the distribution of the densities was produced and used to determine the modal density. Figure 3 shows a sampling of these histograms selected to represent changes in density distributions with cone height. While the distributions appear somewhat irregular, especially those showing lower cone sample densities, most histograms are unimodal with a peak density of ~1.2 g/cm^3 [74.9 lb/ft^3]. Although irregular, the lower cone sample distributions might be described as bimodal; samples from the lowermost upper cone deposits (32407-7) and the uppermost upper cone deposits (32407-1B) show bimodality more prominently. Thus, material produced during the opening and closing stages of the violent Strombolian phase of the eruption is characterized by two distinct clast populations: (i) a low density group with a modal value similar to many of the samples with a unimodal distribution {~1.2 g/cm^3 [74.9 lb/ft^3]} and (ii) a high density group with a modal value of ≥2.0 g/cm^3 [124.9 lb/ft^3].

The mean and peak density for each sample versus cone height for both the upper and lower cone facies are plotted on Figure 4. Minimum density refers to an average of the three minimum density values, and maximum refers to the average of the three highest values. The range of density values present in each sample, or the difference between the highest density clast and lowest density clast per sample, is also plotted. For each of the two episodes represented by the two facies, the range decreased following their initiation, held somewhat steady, and finally increased toward their respective terminations. These trends are mirrored in the maximum density values.

At some sample locations, thick sequences of material could be divided and sampled by clast size. For example, at 32407-5 [Figure 2(c)], three separate samples were collected from a coarse-fine-coarse sequence (A, B, and C, respectively). Similar variations in grain size are seen at other locations but on a smaller scale {e.g., 51207-7 [Figure 2(d)]}. Sample 51207-7A was collected from a bed that coarsened upwards and has a unimodal density distribution (Figure 3) with a peak at 1.2 g/cm^3 [74.9 lb/ft^3]. The density distribution for 32407-5B is markedly dissimilar to 51207-7A (Figure 3), but if the data for 32407-5B and 5C are combined to

represent one coarsening upward bed, the 32407-5B+C distribution is also unimodal with a peak at 1.2 g/cm^3 [74.9 lb/ft^3].

3.2 Microtextures

3.2.1 Vesicles

Upper Cone

From the nine cone samples that included clasts from which thin sections were produced, seven were collected from the upper cone facies, and from these seven, low density, high density, peak density, and transitional density clasts were targeted as representative. These thin sections were studied at high magnifications to discern signature microtextures, including dominant vesicle shapes and sizes. The largest bubble size per clast varies markedly between the low and high density clasts; the low density clasts have a significant population of large bubbles and overall appear well vesiculated compared to the small bubbles present in the poorly vesiculated, high density clasts (Figure 5). Signs of bubble coalescence appear in most clasts, but they are more abundant and obvious in lower density clasts, as seen in Figure 6(a): (i) amoeba-shaped bubble trains, (ii) very thin but intact glass films separating two bubbles just prior to coalescence, and (iii) remnants of glass films indicative of incomplete wall retraction just after bubble combination. Textures dominated by bubble coalescence signatures are created when the magma fragments and quenches as the bubbles are still combining (Klug, et al., 2002). Bubble collapse seems to overprint bubble coalescence in higher density clasts; bubbles in high density sections lose concavity along their walls and have an overall squashed appearance [Figure 6(c)], which is created when pathways have been established through the magma that allow gas to escape prior to fragmentation but largely concurrent with solidification (Mongrain, et al., 2008). The densest clasts with the strongest bubble collapse overprints occur in the lowermost upper cone deposits (Figure 5). These highest density clasts {~2.4 g/cm^3 [149.8 lb/ft^3] or greater} are largely absent from the mid-portion of the upper cone deposits but reappear at the top (Figure 5).

Textural mingling is apparent in most thin sections but most prominently in midrange density clasts (i.e., regions with different dominant vesicle and/or microlite populations distinguishable by size and shape are heterogeneously dispersed throughout the thin section). These regions can sometimes be discerned by studying the microlites but are always identifiable by examining the vesicles, and in some cases, vesicles appear crushed along the boundary. The whole-clast density of some of these midrange density clasts are in fact the result of one clast consisting of regions that appear well vesiculated, similar to the low density clasts, mixed with regions that appear poorly vesiculated, similar to the high density clasts. Mingling can be categorized into three types. In the first type, different regions appear to be distinct, smaller clasts incorporated into a larger, 8 to 32-mm [0.3 to 1.3-in]-diameter clast [Figures 5(b) and 7]. Large vesicles can usually be found along part of the boundary of the smaller clast, and where no boundary vesicle(s) exists, a distinction between the smaller, incorporated clast and the enveloping magma is visible in the microlites. For the second type, domains dominated by smaller bubbles are ubiquitously interspersed in a clast dominated by comparatively larger bubbles [Figures 5(g),(h),(i),(k),(l), and 8]. The edges of these domains are not distinctly marked by bubbles residing along the boundary, and often the domains are either indistinguishable by their microlite populations (i.e., microlites appear homogeneous throughout the whole clast) or only a subtle variation is detectable. In the third characterization of mingling, swaths of smaller vesicles form bands or perimeters within a matrix of comparatively larger vesicles, giving the appearance of a clast within a clast [Figures 5(c),(k), and 9]. A clast from a sample collected at

site 51207-6 exemplifies this type of mingling, but the microlites in this clast show no differences between vesicle bands [Figures 5(c) and 9(c)]. Although not as prominent, a clast from a sample collected at site 32407-7 also shows clast-within-clast textural bands, and the boundary between these bands can easily be discerned when examining its microlites [Figures 5(k) and 9(f)].

Many clasts with peak-mean densities {~1.2–1.6 g/cm^3 [74.9–99.9 lb/ft^3]} show at best only subtle signs of textural mingling. Their measured densities are instead the result of midlevel vesiculation (i.e., they are moderately vesiculated and dominated by medium-sized bubbles) and not the result of a mixture of low and high density textures. These textures are frequently found in the middle of the upper cone beds, sandwiched between the lowermost and uppermost deposits. The bulk of the cone consists of the upper cone facies, which was deposited during the same activity that supported an eruption plume. Thus, upper cone material occupied the same conduit as fallout material. Lathrop Wells fall deposits have finer grain sizes than Lathrop Wells cone deposits, so collecting clasts 8–32 mm [0.3–1.3 in] in diameter was difficult. The ~50 fall deposit clasts measured for density showed a very strong peak at 1.2 g/cm^3 [74.9 lb/ft^3], which is comparable to the peak densities of the cone counterparts. A thin section of a fall deposit scoria clast with a density of 1.2 g/cm^3 [74.9 lb/ft^3] was produced and strongly resembles cone deposit scoria clasts with peak densities and midlevel vesiculation [Figures 5(f) and (p)]. These cone deposit clasts seem to have been produced by efficient ascent and fragmentation processes similar to those that supported the eruption plume.

Lower Cone

Thin sections were made from clasts belonging to two cone samples collected from the lower/early cone facies. Many of the textural features described previously for upper cone clasts are also seen in lower cone clasts (e.g., coalescence and collapse signatures, textural mingling, etc.). One noticeable difference that distinguishes the early cone beds is a population of large, outsized bubbles in the low density clasts in each sample [Figure 5(m)]. This population of bubbles is barely present in the low density clasts belonging to the lowermost deposits in the upper cone and disappears completely with increasing elevation in the upper cone. Also noteworthy in some of the higher density clasts in the lower cone samples are diktytaxitic textures. These actually occur throughout the cone deposits but are most pronounced in samples collected from the lower cone (Figure 10).

3.2.2 Microlites

As described in Perry and Straub (1996), Valentine, et al. (2007), and Vaniman and Crowe (1981), Lathrop Wells basalts are sparsely porphyritic with olivine as the major phenocryst phase and a groundmass assemblage dominated by plagioclase and including minor amounts of olivine, clinopyroxene, and iron-titanium oxides. The plagioclase microlites are generally tabular laths ≤100 µm [3.9×10^{-3} in] measured along their long dimension (Figures 6–10); other phases are considerably smaller {≤25 µm [9.8×10^{-4} in]}. Based on the apparent relative abundance of microlites and glass, groundmass textures appear to be hypocrystalline to hypohyaline. As stated previously, with increasing density, many of the clasts demonstrate a diktytaxitic texture in which plagioclase microlites protrude into voids [Figures 8(d) and 10(d)]. Microlite crystallization does not seem to be correlated to the textural domains defined by the vesicles or to density, and this variability applies to samples collected from both the lower and upper cone. To define boundaries of textural domains, differences in microlite populations can sometimes be used [Figures 7 and 9(f)], whereas in other clasts, boundaries cannot be delineated within the microlites [Figures 8(b) and 9(c)], and neither of these cases coincide with

a particular type of textural mingling (incorporation of smaller clasts, separate domains, or bands). In terms of density, degree of vesiculation and size of bubbles directly relates to whole clast density, but abundance and size of microlites is highly variable. Figure 6 shows an example in which a lower density clast within one sample has a glassier matrix than a higher density clast from the same sample, but in Figure 10, a lower density clast has a hypocrystalline texture.

4 DISCUSSION

Strombolian explosions occur when slug flow dominates conduit ascent; explosions are the result of slugs or large pockets of gas formed by the coalescence of exsolved bubbles that largely fill the width of the conduit bursting at the top of the magma column and occur most commonly in low viscosity magmas, such as basalts (Blackburn, et al., 1976). The term "Strombolian" is often used as a catch-all phrase to describe a wide range of activity seen at the surface, but typical Strombolian activity describes mild, discrete explosions. If the explosions are closely spaced in time, however, the activity appears continuous and can sustain an eruption plume while simultaneously generating lava flows—behavior often associated with Hawaiian-style eruptions. Unlike Strombolian, Hawaiian activity is often associated with high magma ascent rates and/or an annular flow regime in which gas forms a core surrounded by an annulus of magma along the conduit walls (Vergniolle and Mangan, 2000). Parfitt (2004) and Parfitt and Wilson (1995) suggest that basaltic eruptions which exhibit facets of both Hawaiian and Strombolian activity are best described as transitional eruptions. On the higher intensity side of Strombolian, a violent Strombolian eruption style might also represent a transitional flow regime between Strombolian and Plinian eruption styles that marries annular flow (which might itself be caused by rapid-fire slug flow) with dispersed flow in which the continuous phase is gas that carries fragments of magma.

Valentine, et al. (2007, 2005) attribute the distinction between the lower cone and the upper cone deposits (and associated fallout) at Lathrop Wells to changing eruptive styles and therefore changing processes that governed eruption dynamics. The lower cone grew through Strombolian explosions along a short fissure. Differential cooling along the line source effectively sealed off parts of the fissure and focused activity to a single eruptive conduit and vent. The transition between fissure and conduit ascent was marked by the generation of the upper cone facies. Eruption dynamics changed (namely, eruption intensity increased into a violent Strombolian eruption) so that an eruption column was produced.

Field observations of the lower and upper cone deposits support an interpretation of an eruption, or at least the cone-building event, characterized by a minimum of two phases, the second of which was the result of higher intensity activity. Density data and microscopic textures of pyroclasts produced during each phase, however, reveal conduit dynamics with much greater complexity. Deposits in the lower cone, which represent the beginning of the eruptive sequence, are dominated by agglutinate and partly welded lapilli, ribbons, and bombs and were most likely deposited simultaneously with (or close in time to) the effusion of the south lava flow field; these characteristics epitomize Hawaiian–Strombolian style eruptions. Their density distributions are best described as irregular (Figure 3), but they demonstrate a range fairly consistent with their upper cone counterparts, and their low density clasts contain a population of markedly large, outsized bubbles [Figure 5(m)]. Similar large bubbles are seen in clasts produced during classic Strombolian bursts at Stromboli Volcano, Italy, in 2002 (Lautze and Houghton, 2008, 2007, 2005), but the Lathrop Wells lower cone samples as a whole show a significant population of denser clasts compared to the young Stromboli samples. The denser clasts might be the result of (i) the opening of the fissure/conduit at the start of the surface

activity and (ii) an eruption style that is actually transitional between Hawaiian and Strombolian (Parfitt, 2004), such that annular flow is overprinted by slug flow. Lautze and Houghton (2007, 2005) also described a mingling of textural domains in Strombolian clasts, similar to the mingling apparent throughout the Lathrop Wells clasts.

Textural mingling is still apparent in the upper cone deposits, perhaps indicative of a Strombolian influence, but the nonwelded, fragmented lapilli that dominate these deposits and their coeval fallout strongly suggest a dispersed flow regime existed in the conduit. Compared with basaltic pyroclasts produced during Strombolian bursts in 2002 at Stromboli volcano, Italy (Lautze and Houghton, 2007, 2005), and basaltic pyroclasts produced during a Plinian eruption in 122 BC at Etna volcano, Italy (Sable, et al., 2006), textures in the Lathrop Wells upper cone deposits bear a striking resemblance to the Etna textures but with the mingling seen in the Stromboli clasts. Thus, perhaps some combination of both dispersed and slug flow regimes created complex conduit dynamics and left a Strombolian imprint on the violent Strombolian eruption products that comprise the upper cone.

The variations in scale in the coarsening upward sequences in the upper cone might also testify to this Strombolian–violent Strombolian coupling. Reverse bedding is likely caused by grain avalanching [e.g., 51207-7 in Figure 2(d)], but given (i) the difference in the scale between the coarsening upward sequences at sample sites 32407-5 and 51207-7 [Figures 2(c) and (d)] and (ii) the combined density distribution 32407-5B+C is very similar to the distribution for 51207-7A, these coarsening upward sequences of varying thicknesses might reflect directional variations and/or intensity differences in Strombolian bursts. A microcosm of the sequence (e.g., 51207-7A) would be deposited slightly off axis to the dominant eruption trajectory or by a less energetic burst, whereas higher energy activity might result in a thicker sequence (e.g., 32407-5). The package of continuous reversely graded beds at 51207-7 and the variations in clast size at 32407-5 taken together suggest pulses in eruptive activity and interplay between classic Strombolian bursts and violent Strombolian behavior.

In addition to dynamics of dispersed and slug flow regimes, the progression of textures and densities produced from the start to the end of the second eruptive phase demonstrates changes in the ascent pathway. The first pyroclasts to be erupted during this phase show a bimodal density distribution (Figure 3), with the lower density clasts in these samples having a slightly smaller but still outsized bubble population [Figure 5(j)] similar to the low density clasts in the lower cone samples [Figure 5(m)] and the high density clasts having the highest density of any of the measured samples. This diversity, as seen in the range of densities (Figure 4), decreases as cone height increases, and only appears again at the top of the cone in the last material to be erupted. Processes involved in sealing off the fissure and establishing the conduit might explain the density bimodality in the first upper cone beds deposited; magma ultimately erupted at the same time could have experienced variations in ascent (slow ascent along the conduit walls or fast ascent closer to the core). As the second phase of the eruption reached its peak intensity, fragmentation in the conduit was at its most efficient and resulted in similar textures between cone and fall pyroclasts. Toward the waning stages of the eruption, the intensity and efficiency would have decreased, and the variability in the residence times of erupting material could have increased.

5 SUMMARY

This study focused on characterizing conditions of magma ascent during the eruption of Lathrop Wells volcano using the pyroclastic microtextures of eruptive products, especially concentrating on the cinder cone. Salient points include

- Based on the degree of welding and fragmentation seen in the cone deposits at Lathrop Wells volcano, the explosive activity occurred in two phases. Hawaiian–Strombolian eruptive behavior produced the early/lower cone facies, and following the establishment of a focused conduit, eruption intensity increased so that the later/upper cone facies was deposited during violent Strombolian activity.

- Density data and microtextures paint a more complicated picture of the conduit environment than simple slug flow during the first phase and dispersed flow during the second phase. The wide range in densities per sample, the population of outsized bubbles in some of the low density clasts, the population of very dense clasts in some of the samples, the textural mingling, and the simultaneous production of lava flows and/or a sustained eruption plume point toward lower cone growth during a transitional flow regime between slug flow and annular flow and upper cone growth during a flow regime characterized by an interplay between slug flow and dispersed flow. Perhaps the slug–annular pairing resulted from slugs ascending with great rapidity so that individual slug bursts could no longer be discerned. As the eruption progressed and intensity increased, fragmentation might have occurred, and a dispersed flow developed within the core of the conduit. Comparatively, Lathrop Wells pyroclastic textures appear to be a link between 2002 Stromboli textures (slug flow) and 122 BC Etna textures (dispersed flow).

- Lathrop Wells pyroclasts contain abundant signatures of bubble coalescence and collapse in low and high density clasts, respectively. Coalescence suggests the viscosity of the magma was relatively low and the ascent rate slow enough that bubbles could rise within the magma and interact. Collapse implies open pathways permitted degassing and is often associated with denser material traveling nearer the cooler conduit walls.

- Textural mingling is apparent in clasts collected throughout the Lathrop Wells cinder cone. In 2002 Stromboli samples, mingling is attributed to variations in ascent history for magma that ultimately reaches the same free surface. Magma ascending close to the conduit walls that has more time to degas becomes denser and is carried out of the conduit by fragments of lower density, slug-enclosing material when a gas blister bursts (Lautze and Houghton, 2005). Thus, mingling suggests Strombolian processes overprinted eruption dynamics at Lathrop Wells.

- Although microlite size and assemblage is fairly consistent throughout the Lathrop Wells pyroclasts, their abundance varies considerably and is not correlated to clast density or eruptive sequence. Thus, the increase in eruption intensity from the early cone to the later cone was not linearly caused by increased crystallization and viscosity.

The conduit-diameter parameter in the volcanic scenario model abstraction in performance assessments for the potential repository at Yucca Mountain, Nevada, is an important factor in estimating the number of failed waste packages and hence, the amount of waste that may be released. To better understand the assumptions and uncertainties in its parameterization,

microtextures of eruption products collected from Lathrop Wells volcano, an analog eruption, were used to discern conditions in the conduit during magma ascent. While field observations paint a generalized picture of Strombolian–violent Strombolian activity, the density data and microtextures indicate that a complex interplay of flow regimes and conduit dynamics occurred during this eruption. These complexities might affect the flow of magma at intersections between a conduit/dike and a drift and the interactions between intruding magma and the engineered barrier system. The Lathrop Wells samples have been compared to samples collected at Stromboli Volcano, Italy, during eruptions characterized by less energetic activity; based on seismic data, the physical properties of the ascending magma at Stromboli and thereby the conduit dynamics undergo rapid changes starting at approximately 250 m [820 ft] below the crater terrace (Chouet, et al., 2003). Given the current depth proposed for the Yucca Mountain repository is 300 m [984 ft] (Sandia National Laboratories, 2007) and the high water content in Lathrop Wells magma, the level at which the waste might reside within a depth range where potentially important changes occur to ascending magma.

6 REFERENCES

Bechtel SAIC Company, LLC. "Characterize Framework for Igneous Activity at Yucca Mountain, Nevada." ANL–MGR–GS–000001. Rev. 02. Las Vegas, Nevada: Bechtel SAIC Company, LLC. 2004.

Blackburn, E.A., L. Wilson, and R.S.J. Sparks. "Mechanisms and Dynamics of Strombolian Activity." *Geological Society [London] Journal*. Vol. 132. pp. 429–440. 1976.

Cashman, K. "Volatile Controls on Magma Ascent and Eruption." *The State of the Planet: Frontiers and Challenges in Geophysics*. 2003 General Assembly of International Union of Geodesy and Geophysics, Sapporo, Japan. Geophysical Monograph 150. Vol. 19. Washington, DC: American Geophysical Union. pp. 109–124. 2004.

Cashman, K.V., B. Sturtevant, P. Papale, and O. Navon. "Magmatic Fragmentation." *Encyclopedia of Volcanoes*. H. Sigurdsson, ed. New York City, New York: Academic Press. pp. 421–430. 2000.

Chouet, B., T. Ohminato, M. Martini, G. Saccorotti, F. Giudicepietro, G. De Luca, G. Milana, and R. Scarpa. "Source Mechanisms of Explosions at Stromboli Volcano, Italy, Determined From Moment-Tensor Inversions of Very-Long-Period Data." *Journal of Geophysical Research*. Vol. 108. pp. 1–25. 2003.

Fleck, R.J., B.D. Turrin, D.A. Sawyer, R.G. Warren, D.E. Champion, M.R. Hudson, and S.A. Minor. "Age and Character of Basaltic Rocks of the Yucca Mountain Region, Southern Nevada." *Journal of Geophysical Research*. Vol. 101. pp. 8,205–8,227. 1996.

Heizler, M.T., F.V. Perry, B.M. Crowe, L. Peters, and R. Applet. "The Age of the Lathrop Wells Volcanic Center: An $^{40}Ar/^{39}Ar$ Dating Investigation." *Journal of Geophysical Research.* Vol. 104. pp. 767–804. 1999.

Houghton, B.F. and C.J.N. Wilson. "A Vesicularity Index for Pyroclastic Deposits." *Bulletin of Volcanology*. Vol. 51. pp. 451–462. 1989.

Klug, C., K.V. Cashman, and C.R. Bacon. "Structure and Physical Characteristics of Pumice From the Climatic Eruption of Mount Mazama (Crater Lake), Oregon." *Bulletin of Volcanology*. Vol. 64. pp. 486–501. 2002.

Lautze, N.C. and B.F. Houghton. "Single Explosions at Stromboli in 2002: Use of Clast Microtextures to Map Physical Diversity Across a Fragmentation Zone." *Journal of Volcanology and Geothermal Research*. Vol. 170. pp. 262–268. 2008.

———. "Linking Variable Explosion Style and Magma Textures During 2002 at Stromboli Volcano, Italy." *Bulletin of Volcanology*. Vol. 69. pp. 445–460. 2007.

———. "Physical Mingling of Magma and Complex Eruption Dynamics in the Shallow Conduit at Stromboli Volcano, Italy." *Geology*. Vol. 33. pp. 425–428. 2005.

Luhr, J.F. and T.B. Housh. "Melt Volatile Contents in Basalts From Lathrop Wells and Red Cone, Yucca Mountain Region (SW Nevada): Insights from Glass Inclusions." *Eos Transactions*. American Geophysical Union 83 (Abstract V22A–1221). 2002.

Mongrain, J., J.F. Larsen, and P.L. King. "Rapid Water Exsolution, Degassing, and Bubble Collapse Observed Experimentally in K-Phonolite Melts." *Journal of Volcanology and Geothermal Research*. Vol. 173. pp. 178–184. 2008.

Nicholis, M.G. and M.J. Rutherford. "Experimental Constraints on Magma Ascent Rate for the Crater Flat Volcanic Zone Hawaiite." *Geology*. Vol. 32. pp. 489–492. 2004.

Parfitt, E.A. "A Discussion of the Mechanisms of Explosive Basaltic Eruptions." *Journal of Volcanology and Geothermal Research*. Vol. 134. pp. 77–107. 2004.

Parfitt, E.A. and L. Wilson. "Explosive Volcanic Eruptions: IX. The Transition Between Hawaiian-Style Lava Fountaining and Strombolian Explosive Activity." *International Journal of Geophysics*. Vol. 121. pp. 226–232. 1995.

Perry, F.V. and K.T. Straub. "Geochemistry of the Lathrop Wells Volcanic Center." LA–13113–MS. Los Alamos, New Mexico: Los Alamos National Laboratory. 1996.

Sable, J.E., B.F. Houghton, P. Del Carlo, and M. Coltelli. "Changing Conditions of Magma Ascent and Fragmentation During the Etna 122 BC Basaltic Plinian Eruption: Evidence From Clast Microtextures." *Journal of Volcanology and Geothermal Research*. Vol. 158. pp. 333–354. 2006.

Sandia National Laboratories. "Characterize Eruptive Processes at Yucca Mountain, Nevada" ANL–MGR–GS–000002. Rev. 03. ACC: DOC.20070301.0001. Las Vegas, Nevada: Sandia National Laboratories. 2007.

Valentine, G.A., D.J. Krier, F.V. Perry, and G. Heiken. "Eruptive and Geomorphic Processes at the Lathrop Wells Scoria Cone Volcano." *Journal of Volcanology and Geothermal Research*. Vol. 161. pp. 57–80. 2007.

Valentine, G.A., D.J. Krier, F.V. Perry, and G. Heiken. "Scoria Cone Construction Mechanisms, Lathrop Wells Volcano, Southern Nevada, USA." *Geology*. Vol. 33. pp. 629–632. 2005.

Vaniman, D. and B. Crowe. "Geology and Petrology of the Basalts of Crater Flat: Applications to Volcanic Risk Assessment for the Nevada Nuclear Waste Storage Investigations." LA–8845–MS. Los Alamos, New Mexico: Los Alamos National Laboratory. 1981.

Vergniolle, S. and M. Mangan. "Hawaiian and Strombolian Eruptions." *Encyclopedia of Volcanoes*. H. Sigurdsson, ed. New York City, New York: Academic Press. pp. 447–461. 2000.

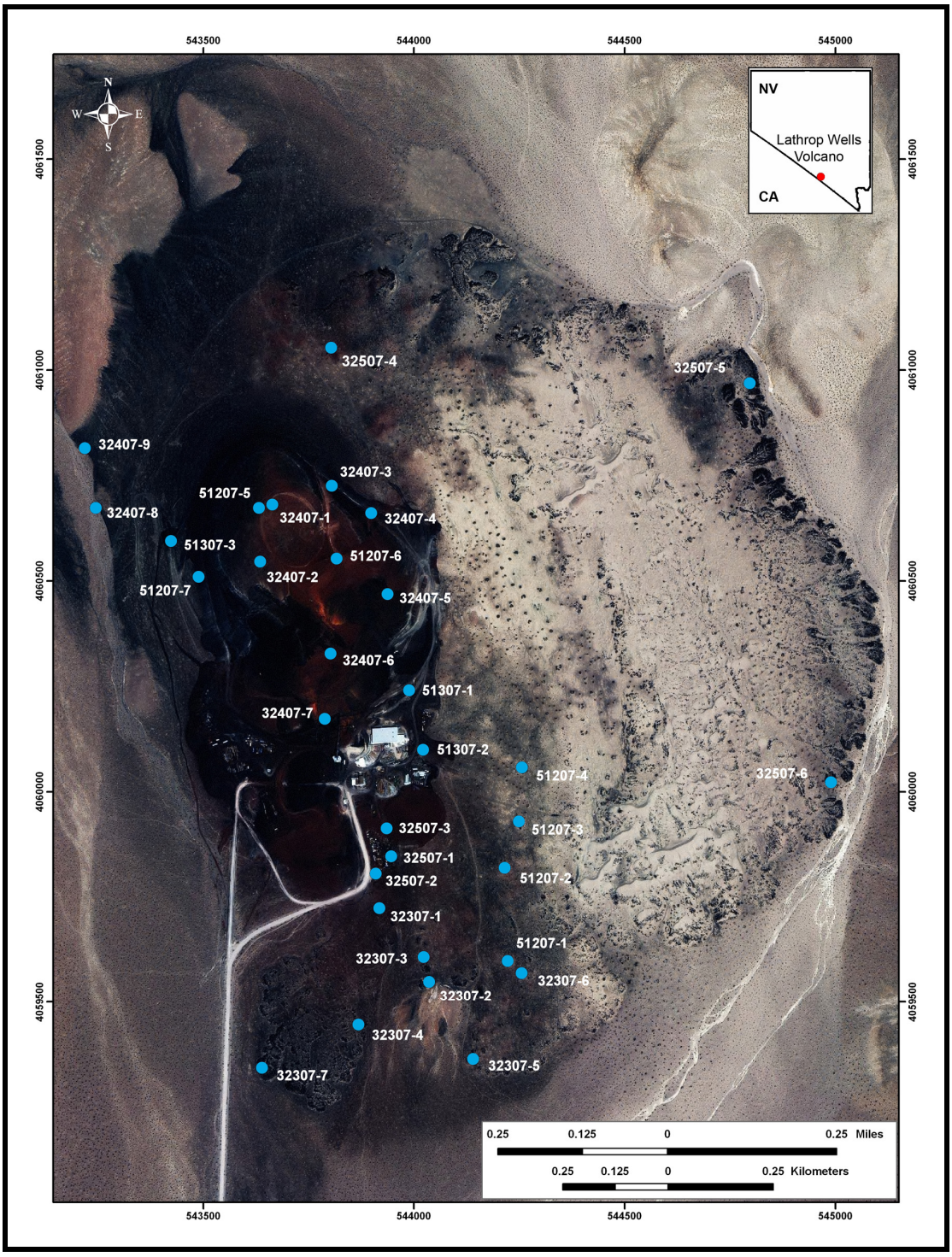

Figure 1. IKONOS® Image of Lathrop Wells Cinder Cone in Nevada. Projection Is UTM, Zone 11, Meters, and Datum is NAD83. One Meter Panchromatic Sharpened Multispectral Dataset Provided by Space Imaging; Image Mosaic by EarthSat Corporation. Sampled Sites Are Marked in Blue.

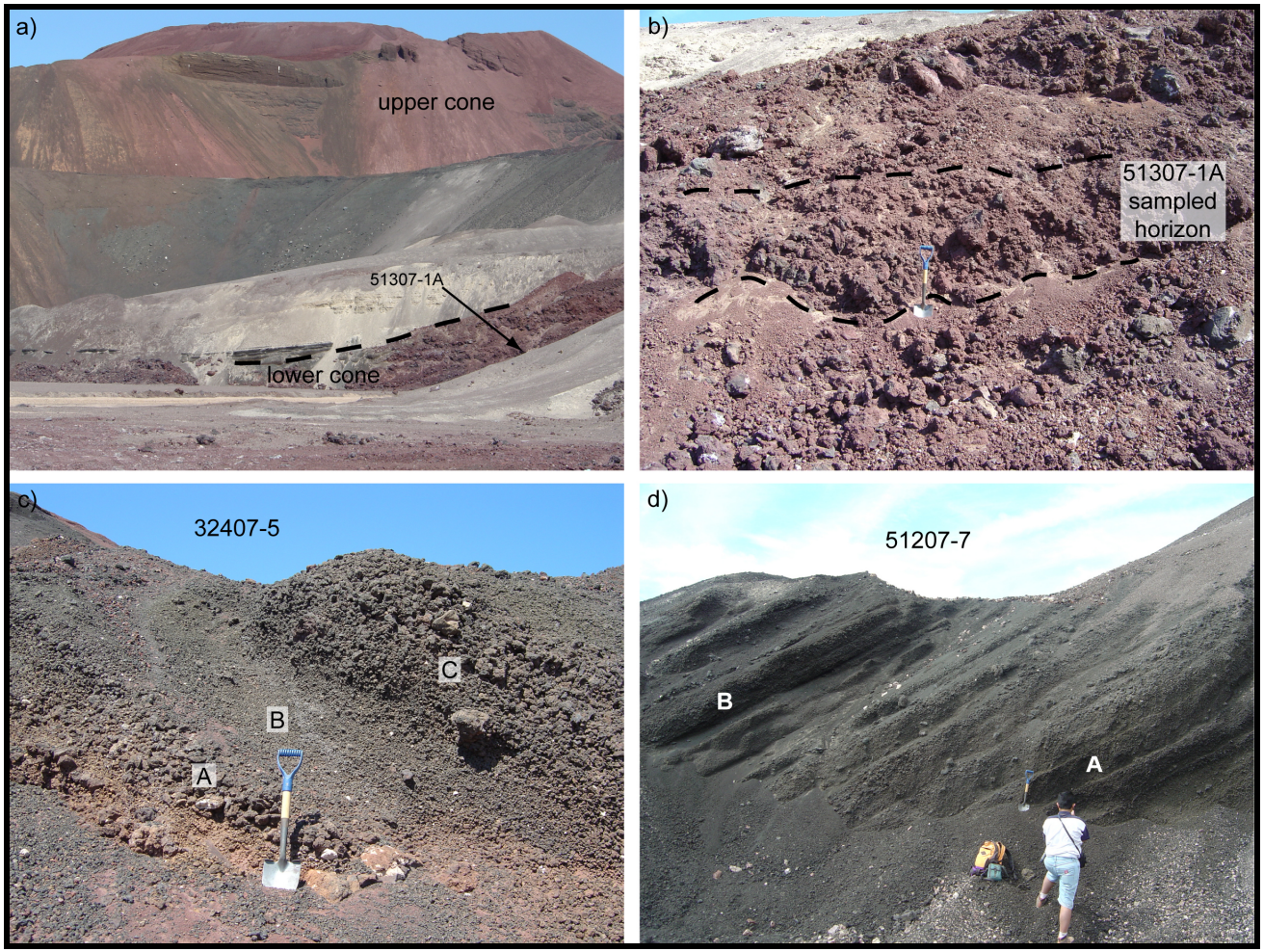

Figure 2. Beds in the Cone Deposits Were Sampled From the Base to the Summit. (a) The Cone Can Be Divided Into Two Facies: the Early/Lower Facies and the Later/Upper Facies. (b) Lower Cone Material Consists of Partly Welded Coarse Lapilli, Ribbons, and Bombs. (c) Highly Fragmented, Upper Cone Samples Were Collected Based on Variations in Grain Size. (d) Package of Reversely Graded Horizons in Upper Cone Material Suggests Grain Avalanching Occurred. In (c) and (d), Capital Letters Indicate Individual Horizons From Which a Sample Was Collected.

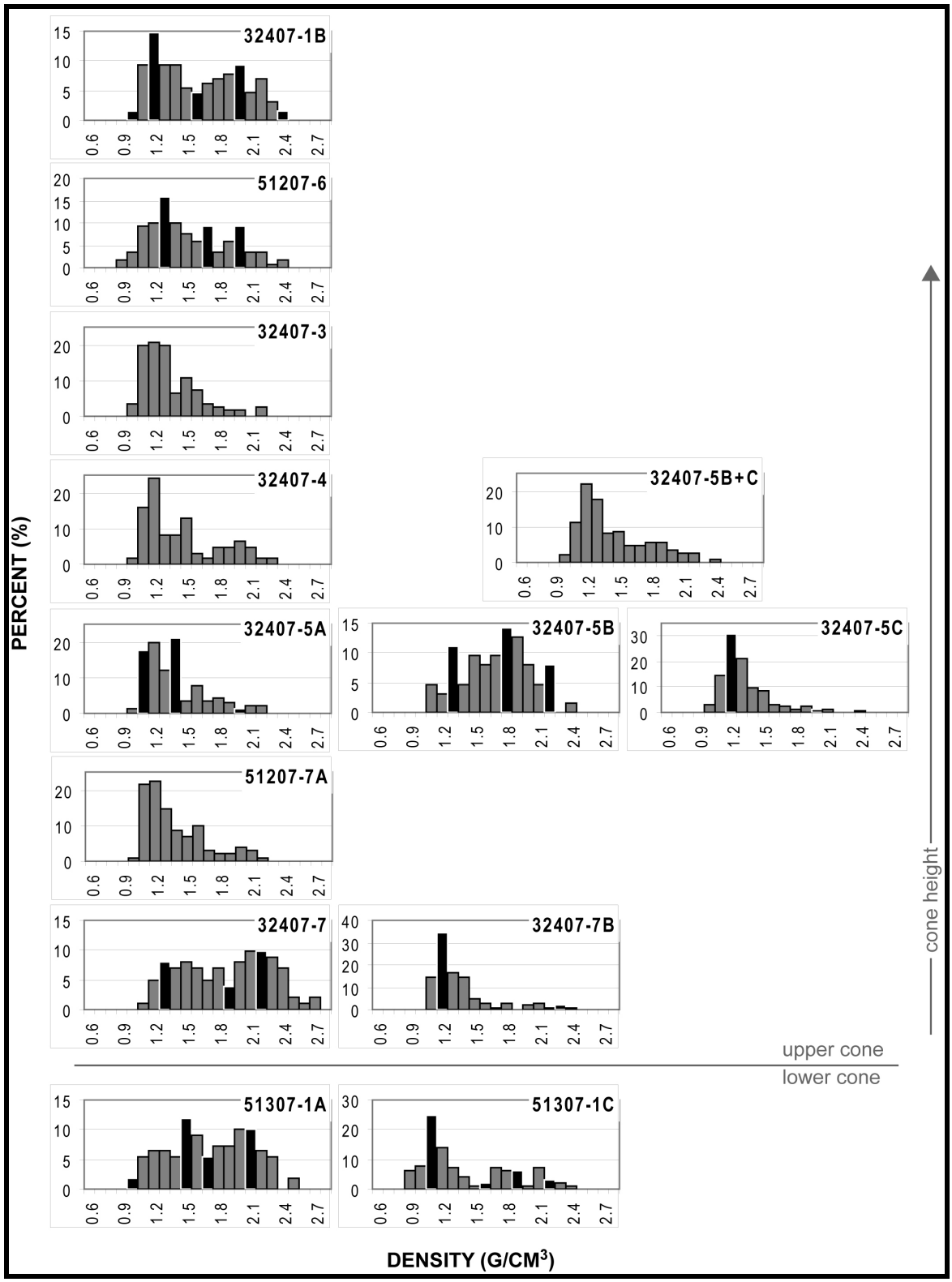

Figure 3. Histograms Depicting the Density Distributions for Selected Samples. The Densities of Clasts Used for Image Analysis Are Shown in Black.

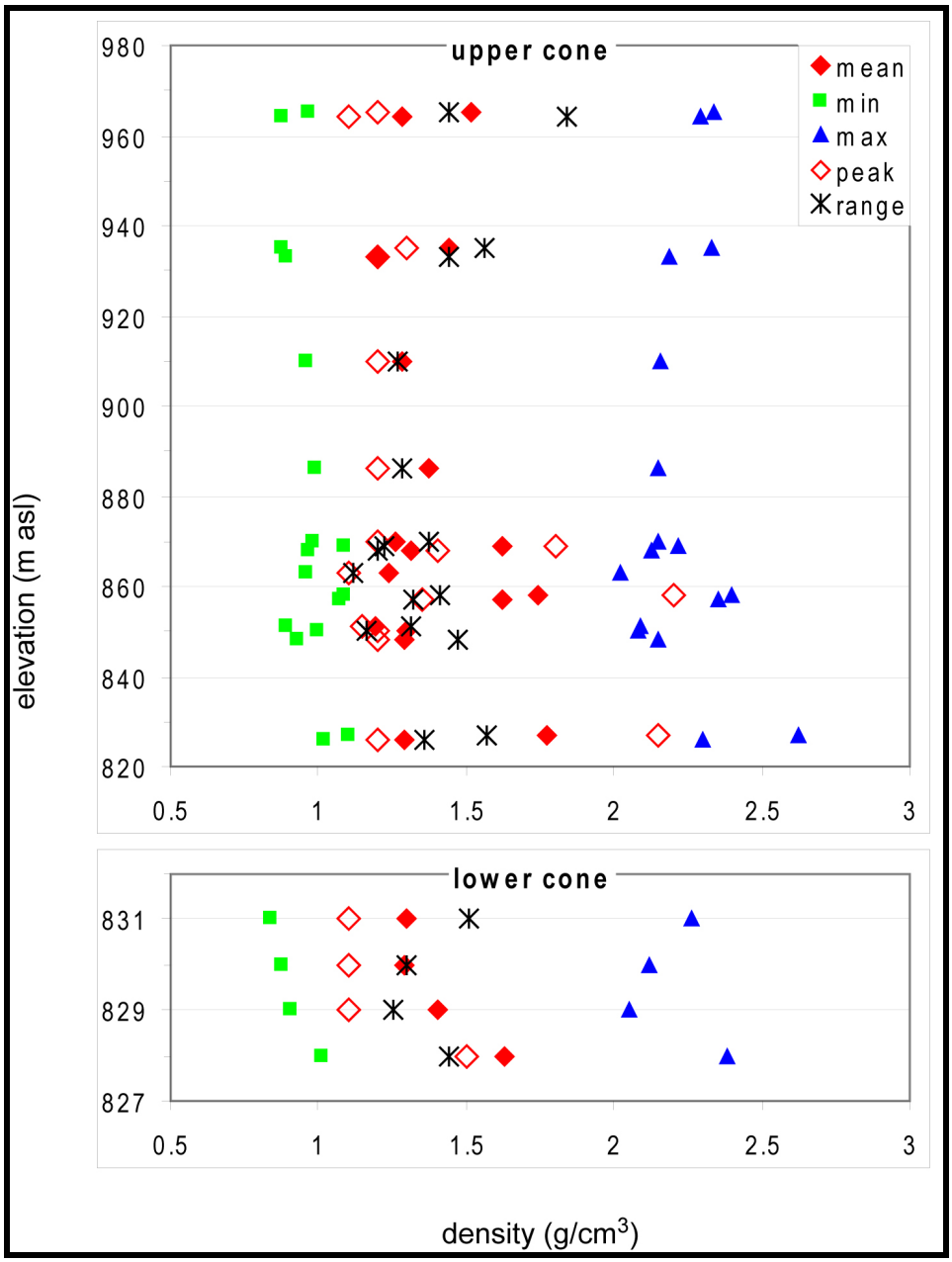

Figure 4. Plot of Sample Densities Against Cone Height. *Min* Is the Average of the Three Minimum Density Clasts Per Sample, *Max* Is the Average of the Three Maximum Density Clasts, and *Range* Is the Difference Between the Highest and Lowest Measured Densities Per Sample.

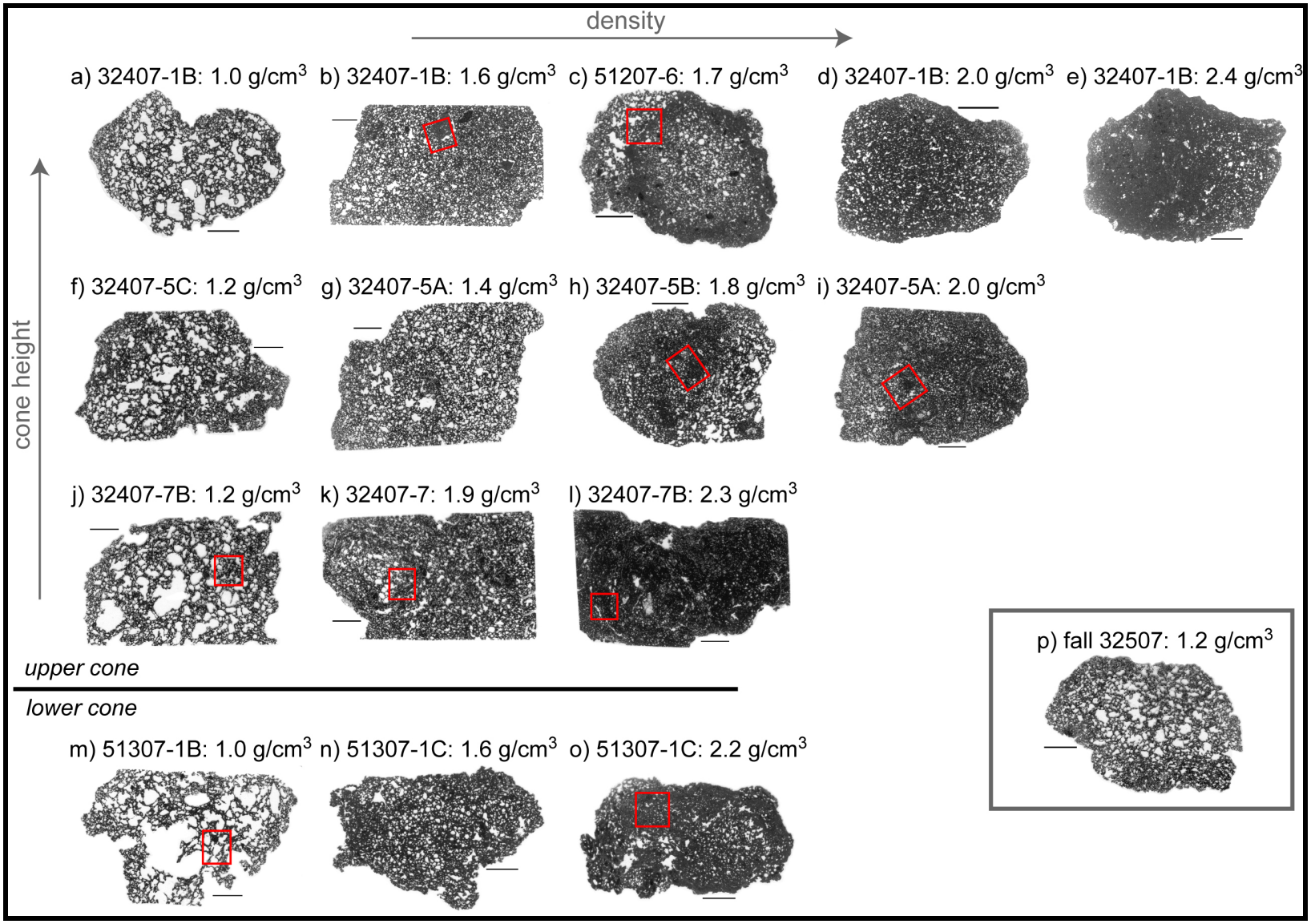

Figure 5. Optically Scanned Images of Thin Sections for Selected Clasts. Vesicles Appear White and the Glass/Crystals Gray-Black. Scale Is 5 mm [0.2 in] in Length. Red Boxes Outline Regions of the Clast Shown at Higher Magnification in Other Figures.

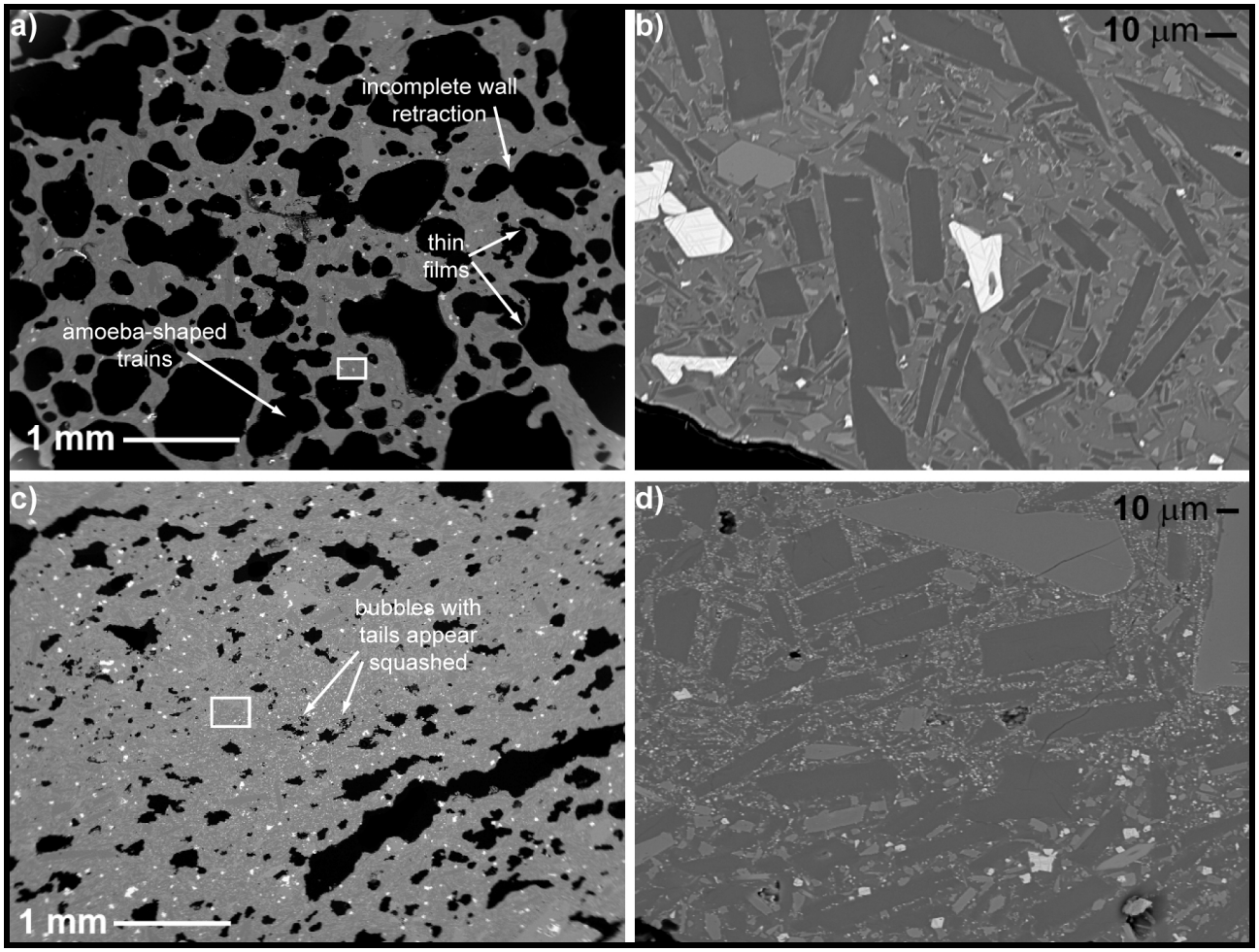

Figure 6. Backscatter Electron Images of Bubble Coalescence in Low Density Clasts (a) and Bubble Collapse in Higher Density Clasts (c). Bubbles Appear Black in These Images. Red Boxes in Figures 5(j) and (l) Outline Areas Captured at Higher Magnification [(a) and (c), Respectively]; White Boxes in (a) and (c) Outline Areas Captured at Higher Magnification [(b) and (d), Respectively]. In This Sample (32407-7B), the Lower Density Clast Has a Glassier Matrix (b) Than the Higher Density Clast (d).

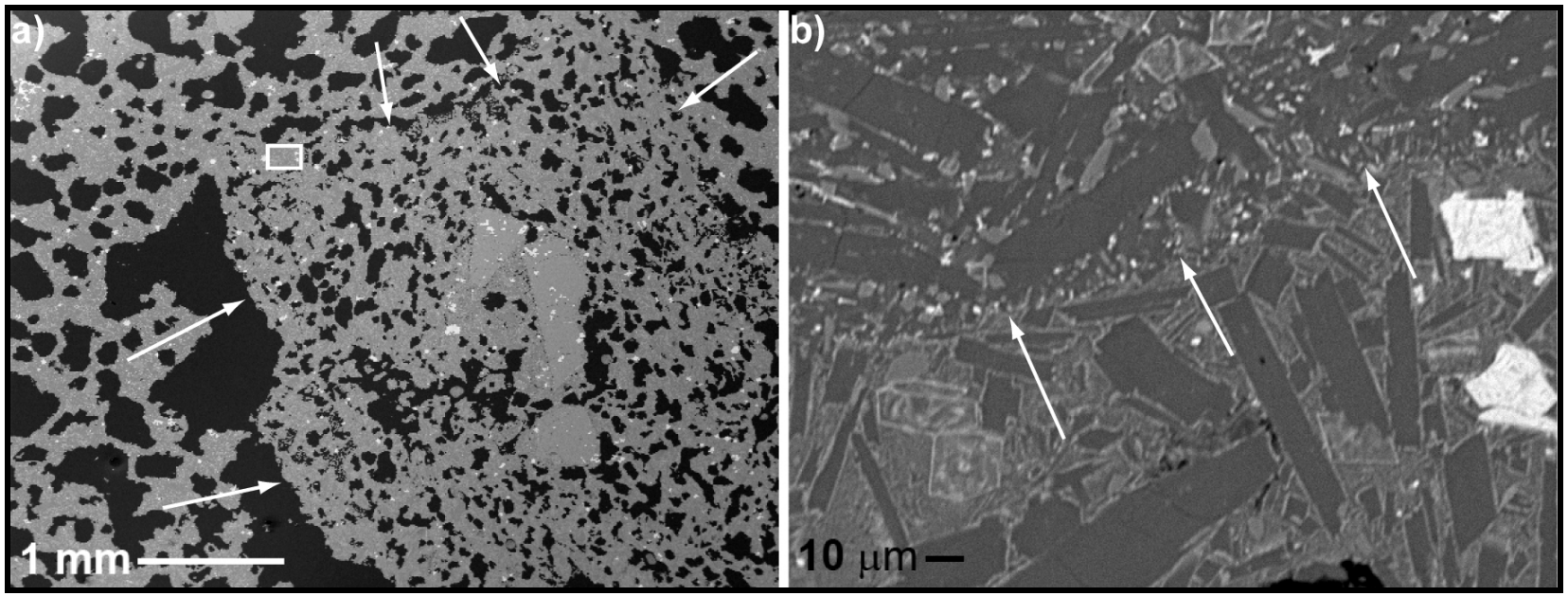

Figure 7. Backscatter Electron Images Showing Incorporation of Distinct, Smaller Clasts Within a Larger Clast. Arrows Point to Boundary, Which Is Visible in Both Vesicle (a) and Microlite (b) Populations. Red Box in Figure 5(b) Outlines Area Captured at Higher Magnification in (a); White Box in (a) Outlines Area Captured at Higher Magnification in (b).

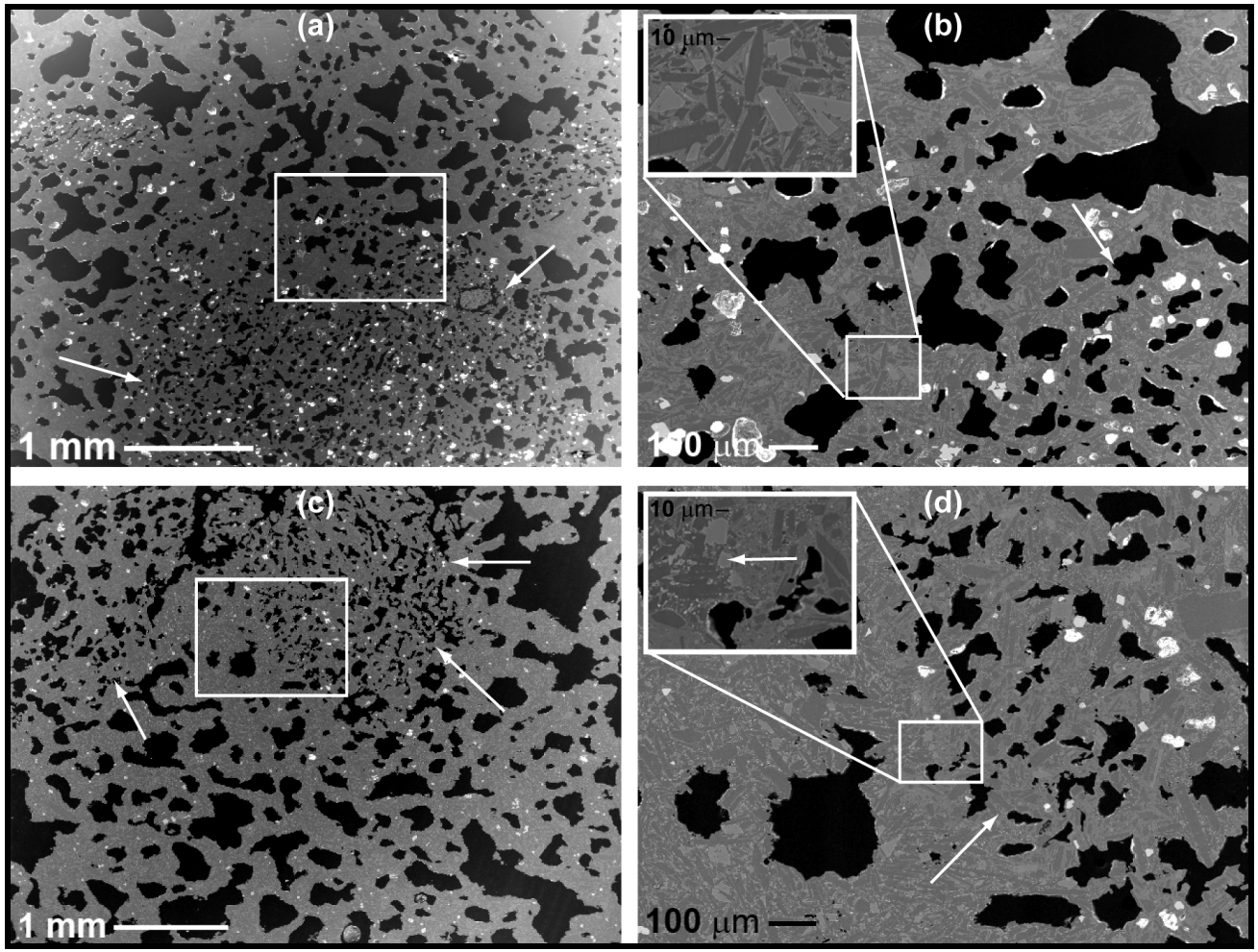

Figure 8. Backscatter Electron Images Showing Mingling of Domains Distinguishable by Vesicle Population. Red Boxes in Figures 5(h) and (i) Outline Areas Captured at Higher Magnification [(a) and (c), Respectively]; White Boxes in (a) and (c) Outline Areas Captured at Higher Magnification [(b) and (d), Respectively]; Regions Within (b) and (d) Are Also Shown at Higher Magnification. Arrows Point to Boundaries. In (b), No Boundary Is Seen in the Microlites Between Domains. In (d), a Subtle Variation in Microlites Exists Between Domains.

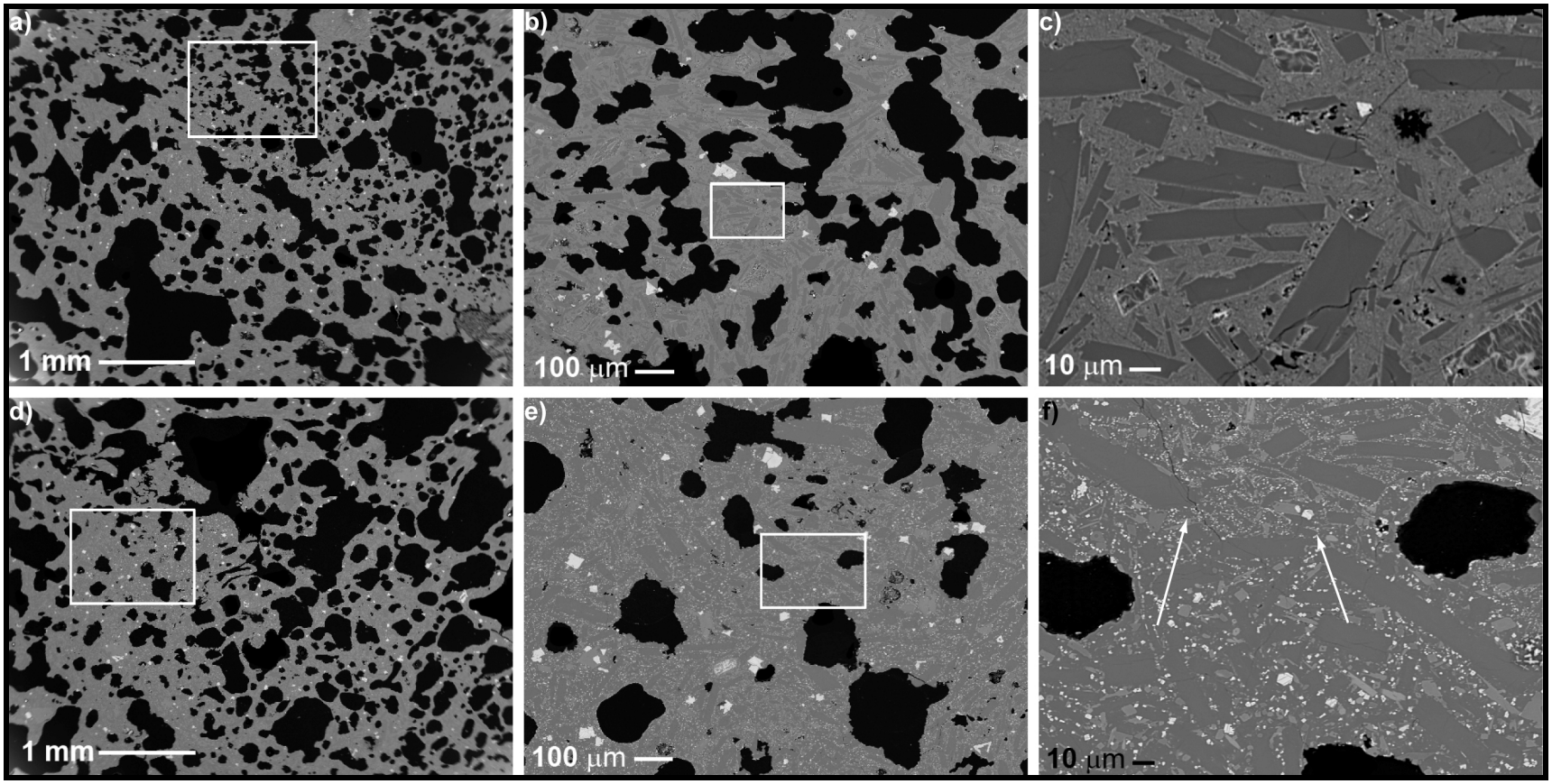

Figure 9. Backscatter Electron Images Taken Within Clasts With Distinct Textural Domains Appearing as Internal Bands or Perimeters. Images (a), (b), and (c) Are From the Clast Shown in Figure 5(c), and (d), (e), and (f) Are From Figure 5(k). White Boxes Outline Areas Captured at Higher Magnification, and Magnification Increases From Left to Right. Arrows Point to Boundary. In (b) and (c), Textural Differentiation Is Not Apparent in the Microlites, and the Clast Has a Glassy Matrix. In (e) and (f), a Definitive Boundary Between Textural Domains Is Apparent in the Microlites, and the Clast Has a Hypocrystalline Matrix.

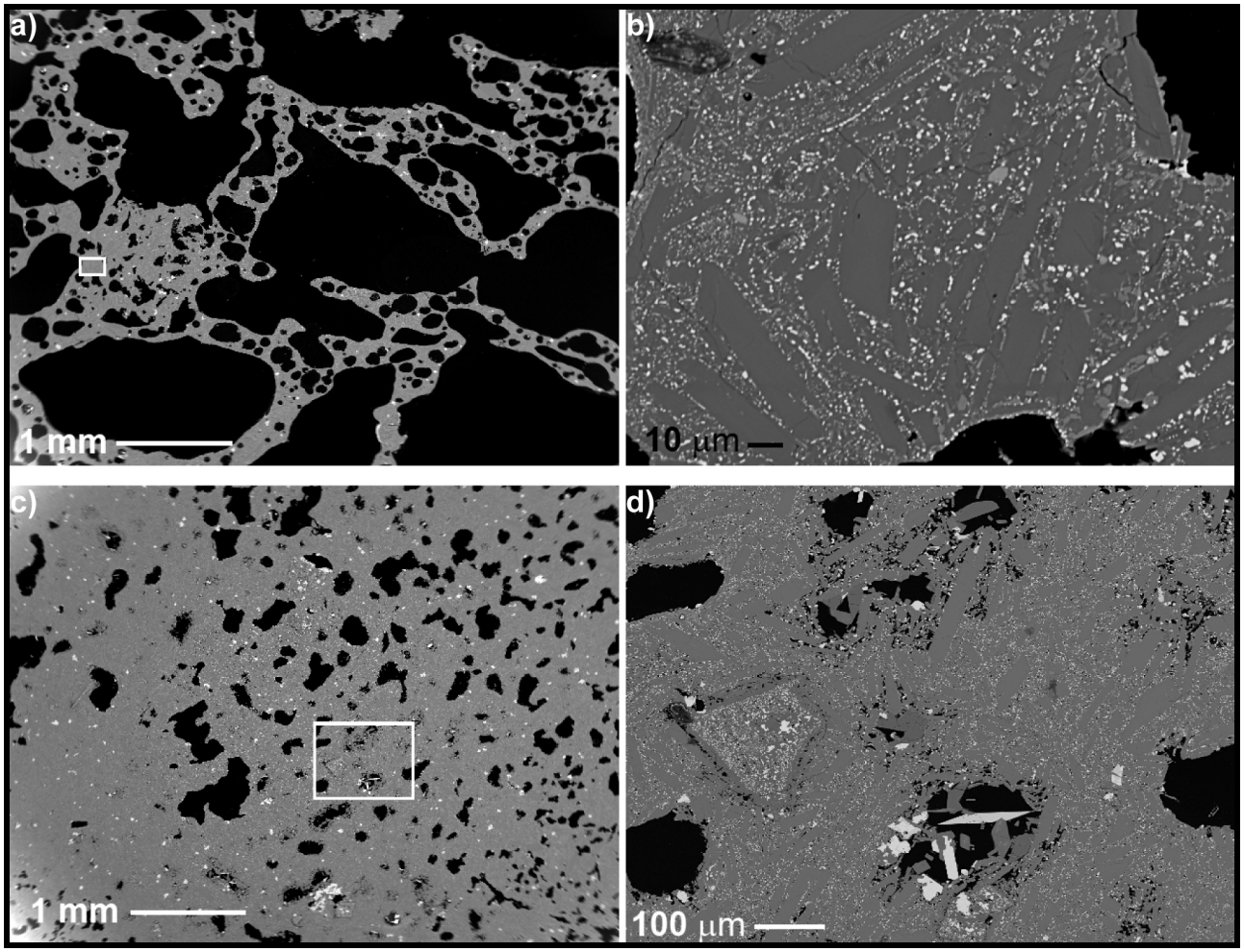

Figure 10. Backscatter Electron Images Demonstrating That the Range of Textures in Lower Cone Samples Is Similar to the Range in Upper Cone Samples. Red Boxes in Figure 5(m) and (o) Outline Areas Captured at Higher Magnification [(a) and (c), Respectively; White Boxes in (a) and (c) Outline Areas Captured at Higher Magnification [(b) and (d), Respectively]. Lowest Density Clasts Contain a Population of Outsized Bubbles and Are Hypocrystalline [(a) and (b)]. Diktytaxitic Textures [(c) and (d)] Appear Prominently.